Synthesis of the metastable α-Al1.8Fe0.2O3 solid solution from precursors prepared by combustion

Anne Cordier, Alain Peigney, Eddy de Grave, Emmanuel Flahaut, Christophe Laurent

Synthesis of the metastable α-$Al_{1.8}Fe_{0.2}O_3$ solid solution from precursors prepared by combustion

Anne Cordier [a], Alain Peigney [a], Eddy De Grave [b], Emmanuel Flahaut [a], Christophe Laurent [a,*]

[a] *CIRIMAT UMR CNRS-UPS-INP 5085, Centre Interuniversitaire de Recherche et d'Ingénierie des Matériaux, Université Paul-Sabatier, 31062 Toulouse cedex 9, France*

[b] *NUMAT, Department of Subatomic and Radiation Physics, University of Ghent, Proeftuinstraat 86, B-9000 Gent, Belgium*

Abstract

The aim of the paper is to synthesise α-$Al_{1.8}Fe_{0.2}O_3$ solid solutions from precursors prepared by the nitrate/fuel combustion synthesis route, using either citric acid or urea, or a mixture of both as the fuel, and different fuel/nitrates ratios. In a first part, global reactions are proposed for each synthesis, which are useful to explain the differences in powder volume, morphology, crystallisation state and specific surface area reported in the second part of the study. In a third part, the powders were further calcined at 1100 °C in order to obtain the corundum form. A combination of Mössbauer spectroscopy, XRD and specific surface area measurements revealed that only the powders prepared with $\Phi_e = 2$ are the desired monophased α-$Al_{1.8}Fe_{0.2}O_3$ solid solutions.

Keywords: Powders-chemical preparation; Combustion synthesis; $(Al, Fe)_2O_3$

1. Introduction

Alumina, α-Al_2O_3 (corundum), has been the subject of numerous investigations due to its important applications in advanced engineering materials. Hematite, α-Fe_2O_3, is often added to alumina to reduce the temperature of the γ-α phase transition, which enables to produce α-Al_2O_3 with a smaller grain size.[1] The addition of hematite to alumina also incites interests in the field of heterogeneous catalysis.[2] Another key feature of alumina/hematite materials is to serve as precursors for the in situ formation of carbon nanotubes (CNTs). Indeed, when α-$Al_{2(1-x)}Fe_{2x}O_3$ solid solutions are reduced in a H_2-CH_4 atmosphere at temperatures between 850 and 1070 °C, iron-containing nanoparticles of a few nanometers in diameter are formed at the surface of the oxide grains, and these immediately catalyse the decomposition of CH_4, resulting in the formation of CNTs within the powder.[3] This method, which obviates any mixing step, is particularly interesting for the subsequent preparation of dense oxide-matrix composites with a very homogeneous distribution of the CNTs.[4–6] It has been shown that the starting solid solution for CNT production must be crystallised in the corundum form[7] and that a partitioning into two phases, α-Al_2O_3 rich (α_1) and α-Fe_2O_3 rich (α_2), respectively, must be avoided.[8] Moreover, to optimise the amount of CNTs, a maximum iron content in the single-phase oxide is desirable. Hence, an amount of iron as closely as possible to the solubility limit of α-Fe_2O_3 in α-Al_2O_3, should be applied. However, although many authors have studied the Al_2O_3–Fe_2O_3 system, the solubility limit of Fe_2O_3 in α-Al_2O_3 at temperature below 1200 °C has remained uncertain, the maximum value being generally estimated to be near 10 mol%, but this value appears difficult to achieve according to the synthesis route.[9–14] The equilibrium phase diagram in Fig. 1 was drawn according to the results reported by Muan and Gee.[9] Thermodynamic calculations by Polli et al.[15] established that a 10 mol% hematite solid solution is supersaturated at room temperature, but these authors also showed that such a metastable solid solution can be obtained at low temperature from liquid precursors, whereas its partitioning is promoted at higher temperatures. Note however that these authors[15] work with very small powder quantities (20 mg). Thus, it appears that the choice of the synthesis route and subsequent heat treatments is crucial for obtaining a truly single-phase α-$Al_{1.8}Fe_{0.2}O_3$ solid

doi:10.1016/j.jeurceramsoc.2005.08.014

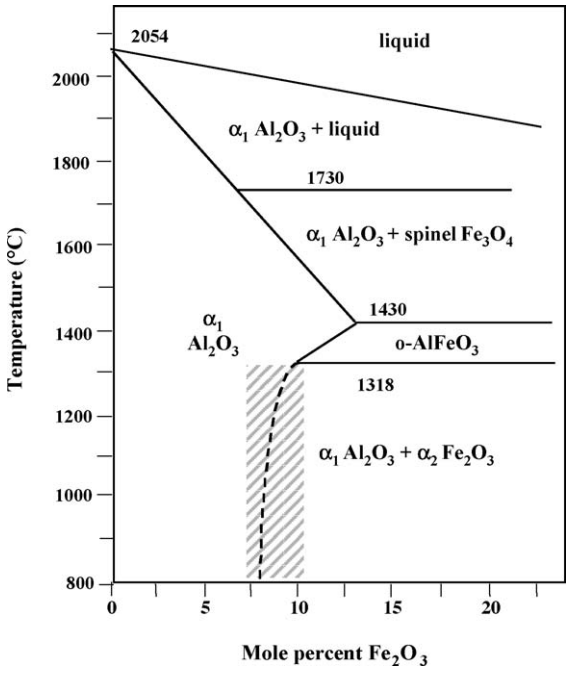

Fig. 1. Part of the phase diagram for the Al_2O_3-Fe_2O_3 system according to the results reported by Muan and Gee.[9] The shaded area reflects the uncertainty on the phase partitioning at lower temperatures.

solution. In this respect, the combustion synthesis is an easy, safe, rapid and economic method used to synthesise various oxides or to prepare multi-component ceramics.[16] The process is based on a rapid redox reaction between a fuel (urea, citric acid, glycine, etc.) and oxidisers (generally metal nitrates), which starts under a moderated heating. This exothermic reaction can produce some fumes and/or a flame. The crystallisation degree of the oxide and its intrinsic characteristics generally depend both on the type of fuel[16–18] and on the fuel/oxidiser ratio.[19–22]

In the present work, we report for the first time on the synthesis of a single-phase α-$Al_{1.8}Fe_{0.2}O_3$ solid solution by heat-treatment of precursors prepared by the combustion route. In particular, we systematically examined the effect of the nature of the fuel (citric acid, urea or a mixture) on the one hand, and of the influence of the ratio (Φ_e) between the total oxidising and reducing valences on the other hand, on the combustion process and on some relevant characteristics (colour, crystallisation state, specific surface area, morphology) of the obtained powders. Further, the temperatures of the amorphous-γ and of the γ-α phase transitions upon heat-treatment, the morphology and composition of the powders and the lattice parameters of the α-$Al_{1.8}Fe_{0.2}O_3$ phase were determined in relation to the chemical conditions of the synthesis procedure.

2. Experimental methods

2.1. Powder synthesis

With the aim to prepare 3 g of α-$Al_{1.8}Fe_{0.2}O_3$ powder, the required proportions of $Al(NO_3)_3$, $9H_2O$ and $Fe(NO_3)_3$, $9H_2O$ were dissolved in the minimum amount of water in a Pyrex dish. The required proportion of fuel, citric acid (noted CA) and/or urea (noted U) was then added under continuous stirring up to complete dissolution. The fuel proportions were calculated by considering the total oxidising valence (VO) and reducing valence (VR) of the different species.[23] The total oxidising valence of the metal nitrates is VO = 30. The reducing valences of CA and U are equal to 18 and 6, respectively. For the CA/U mixtures, VR was calculated as VR = m VCA + n VU with m and n the respective molar quantities calculated so that the so-called stoichiometric ratio Φ_e = VR/VO is equal to unity.[23]

The dish was placed in a furnace preheated at 550 °C, keeping the door of the furnace open. After water evaporation, a combustion reaction takes place according to a redox reaction (1) between the nitrates and fuel(s), producing an oxide powder (henceforward named as-prepared powder):

$$2[0.9Al(NO_3)_3 + 0.1Fe(NO_3)_3] + m(C_6H_8O_7) + n(NH_2\text{-}CO\text{-}NH_2) \rightarrow Al_{2(1-x)}Fe_{2x}O_3 + \text{gas}(N_2, CO_2, H_2O, NO_x, \ldots) \quad (1)$$

However, as discussed by Zhang and Stangle[21], this method involves some approximations. Indeed, the oxidising valence of the air in the atmosphere is not taken into account, which affects VO. The nitrogen-containing products are considered as being only N_2 (and thus zero is taken as the valence of nitrogen element in the calculations), despite that nitrogen oxides and/or NH_3 can be formed in usually undetermined proportions. This affects both VO and VR. Zhang and Stangle[21] have thus proposed that there is a stoichiometric zone around $\Phi_e = 1$ for which the redox conditions are neither too oxidising nor too reducing. For this reason, the syntheses were performed for different values of Φ_e (0.5, 1 and 2). The relevant values of Φ_e, m and n for all syntheses are summarised in Table 1.

The as-prepared powders were then submitted to two thermal treatments in flowing air. The first one (heating at 300 °C h^{-1} up to 550 °C, 1 h of dwell time and natural furnace cooling down to room temperature) aims at oxidising any possible residual carbon in the as-prepared powders. The second one (heating at 300 °C h^{-1} up to 600 °C, then heating at 900 °C h^{-1} up to 1100 °C, 30 min of dwell time and natural furnace cooling down to room temperature) is performed in order to obtain the corundum (α) phase.

2.2. Characterization

All powders (as-prepared, calcined at 550 °C and calcined at 1100 °C) were examined by X ray diffraction (XRD) using Cu Kα radiation (Bruker D4 Endeavor). XRD was performed for phase detection and identification and to determine the unit-cell parameters (Seifert 3003 TT), which were calculated by the Rietveld method using the "Fullprof" software. The specific surface area of the powders calcined at 550 °C and 1100 °C was measured by the BET method (Micrometrics Flow Sorb II 2300) using nitrogen adsorption at liquid nitrogen temperature. Differential thermal analyses (DTA, Netzsch 404S) were car-

Table 1
Description of the phenomena observed during the reaction for powders prepared using only citric acid (CA) or only urea (U) or a mixture of both (CAU) as the fuel, with different fuel/nitrate ratios (Φ_e)

Powder	Φ_e	m CA (mol)	n U (mol)	Combustion phenomena	Powder characteristics
CA0.5	0.5 (100% CA)	0.83	0	Red fumes, thickening and blackening of the solution incandescence	Light yellow and black, 2v
CA1	1 (100% CA)	1.67	0	Red fumes, thickening of the solution, white flame, incandescence	Light yellow and black, 1v
CA2	2 (100% CA)	3.33	0	Red fumes, thickening of the solution, white flame, incandescence	Orange yellow, 2v
U0.5	0.5 (100% U)	0	2.5	Bubbling of the solution, foaming yellow flame	Khaki and red, 3v
U1	1 (100% U)	0	5	Bubbling of the solution, foaming yellow flame, crackling	Greyish and red, 3v
U2	2 (100% U)	0	10	Bubbling of the solution, foaming yellow flame, crackling, ammonia smell	Dark red, 1v
CAU1	1 (50% CA, 50% U)	0.83	2.5	Red fumes, thickening, blackening and foaming, incandescence	Light yellow, 3v
CAU2a	2 (75% CA, 25% U)	2.5	2.5	Red fumes, blackening and very large foaming, incandescence	Light yellow and black, 6v
CAU2b	2 (50% CA, 50% U)	1.67	5	Blackening and large foaming, incandescence	Light yellow and black, 4v
CAU2c	2 (25% CA, 75% U)	0.83	7.5	Blackening and foaming, incandescence, ammonia smell	Yellow, 2v

Since CA and U have a different reducing valence, the molar quantity of CA and U (m and n, respectively) is also indicated. The colour and apparent volume (1v being the smallest and 6v the highest) of the as-prepared powders is reported.

ried out in flowing air on the as-prepared powders (heating at 1200 °C h^{-1} up to 550 °C) and on the powders calcined at 550 °C (heating at 1200 °C h^{-1} up to 1200 °C). The 550 °C-calcined powders were observed by field-emission gun scanning electron microscopy (FEG-SEM, JEOL 6700F). The powders calcined at 1100 °C were studied by ^{57}Fe Mössbauer spectroscopy at room temperature (RT). Selected powders were also studied at 80 K. Mössbauer spectra (MS) were recorded with a ^{57}Co (Rh) source using a conventional time-mode spectrometer with a constant-acceleration drive and a triangular-reference signal. Accumulation of the data was performed in 1024 channels until a background of at least 10^6 counts/channel was reached. The spectrometer was calibrated by collecting at RT the MS of a standard α-Fe foil and the isomer-shift values quoted hereafter are with reference to this standard. The measured absorbers were prepared with the amount of powder corresponding to 10 mg of iron atoms/cm^2. The spectra were generally analysed assuming symmetrical components with Lorentzian line shapes.

3. Results and discussion

3.1. Combustion synthesis

The combustion synthesis is a violent redox reaction during which flames and/or fumes can be produced. The phenomena observed during the reaction and some characteristics of the as-prepared powders (colour, volume) are described in Table 1.

3.1.1. Citric acid combustion (powders CA0.5, CA1 and CA2)

Three syntheses were made with different Φ_e (0.5; 1; 2) producing three as-prepared powders denoted CA0.5, CA1 and CA2, respectively. After water evaporation, a gel-like product was formed, possibly due to polymerisation of the intermediate products.[24] Its drying is accompanied by its blackening and the emanation of red fumes, revealing the production of NO_2, and the beginning of the combustion reaction. This was followed by a long incandescence for CA0.5 and by a white flame itself followed by a long incandescence for CA1 and a shorter one for CA2. All three as-prepared powders are yellowish with some black residues, particularly CA0.5 and CA1. CA1 is about half-less voluminous than CA0.5 and CA2 (Table 1).

Other authors[20,25] have shown that CA forms a complex with metallic cations and so allows a better homogeneity of the solution. However, complexation was not taken into account here because the duration of the present process (dissolving the nitrates and CA in aqueous solution and the combustion reaction) is much shorter (about 20 min) in comparison with over 3 h in Pechini or sol–gel methods[20,25] and no precipitate was observed and because neither pH adjustment nor evaporation process were performed in the present work. Furthermore, this would not fundamentally change the redox reaction.

Hon et al.[26] reported the thermal decomposition in air of CA at a moderate temperature (175 °C):

$$C_6H_8O_7 \rightarrow C_5H_4O_3 + CO_2 + 2H_2O \quad (2)$$

If O_2 is available, the decomposition can further proceed via reactions (3) and (4):

$$C_5H_4O_3 + \tfrac{3}{2}\,O_2 \rightarrow C_4H_2O_3 + CO_2 + H_2O \quad (3)$$

$$C_4H_2O_3 + O_2 \rightarrow 4CO + H_2O \quad (4)$$

Other researchers[20,25] using different amounts of CA and solutions with different pH have shown that the nitrate/CA combustion reaction does not occur below 250 °C when a heating rate of 10 °C min^{-1} is applied. However, since the present experiments are performed in a furnace pre-heated at 550 °C and reaction (2) occurs readily, we suggest that it takes place before the nitrate/CA combustion.

Pacewska et al.[27] have reported that $Al(NO_3)_3, 9H_2O$ decomposes in two steps, a first one below 170 °C and a second one above 170 °C, and further showed that the nitrate IR-absorption band is still very strong at 200 °C. Considering the present heating conditions, it is proposed that there is no decomposition of the nitrates prior to the combustion. The decomposition of the aluminium and iron nitrates is represented by the following reaction:

$$2M(NO_3)_3 \rightarrow M_2O_3 + 6\,NO_2 + \tfrac{3}{2}O_2 \quad (5)$$

This reaction (5) produces NO_2 and the characteristic red fumes. Since no release of red fume before the combustion reaction was observed here, one can infer that (5) takes place during the combustion itself. Hence, the redox reaction occurs between the nitrates and $C_5H_4O_3$, thus involving reaction (3) and (5). It is proposed that the O_2 produced by reaction (5) only reacts in the combustion reaction, and that the atmospheric O_2 only (partially) burns the black residues (Table 1) during the end of the incandescence. This is supported by a study[28] showing that there was no change between experiments performed in air and in argon atmosphere.

Reaction (4) can only occur after reaction (3) is completed and enough O_2 has been produced by reaction (5). Consequently, (4) takes place if CA is defective. This is the case for CA0.5, and so the global combustion reaction for CA0.5 can be written as:

$$2M(NO_3)_{3(s)} + \tfrac{5}{6}C_5H_4O_{3(s)} \rightarrow M_2O_{3(s)} + 6NO_{2(g)} + \tfrac{13}{12}H_2O_{(g)} + \tfrac{5}{6}CO_{2(g)} + \tfrac{7}{12}C_4H_2O_{3(s)} \quad (6)$$

For CA1 and CA2, the amount of O_2 produced by reaction (5) is insufficient to complete reaction (3). As a result, reaction (4) does not take place and the global combustion reactions are, respectively

$$2M(NO_3)_{3(s)} + \tfrac{5}{3}C_5H_4O_{3(s)} \rightarrow M_2O_{3(s)} + 6NO_2 + H_2O_{(g)} + CO_2 + \tfrac{2}{3}C_5H_4O_{3(s)} + C_4H_2O_{3(s)} \quad (7)$$

and

$$2M(NO_3)_{3(s)} + \tfrac{10}{3}C_5H_4O_{3(s)} \rightarrow M_2O_{3(s)} + 6NO_{2(g)} + H_2O_{(g)} + CO_{2(g)} + \tfrac{7}{3}C_5H_4O_{3(s)} + C_4H_2O_{3(s)} \quad (8)$$

The black residues in the product correspond to $C_4H_2O_3$ for CA0.5 and to both $C_4H_2O_3$ and $C_5H_4O_3$ for CA1 and CA2. The quantity of gas products as obtained from the global reactions (6)–(8) are moderate and similar (8.9, 8 and 8 mol for CA0.5, CA1 and CA2, respectively), which could explain the low apparent volume of the solid products.

3.1.2. Ureic combustion (powders U0.5, U1 and U2)

The phenomena observed using urea are very different from those observed during combustions using CA (Table 1). Very rapidly after the beginning of water evaporation, a sudden foaming occurs simultaneously with the beginning of the combustion. No red fumes are formed. A yellow flame appears and the combustion is completed within a few tens of seconds. The maximum temperature achieved during urea syntheses is thus probably higher than for CA syntheses. Only for U2 the typical smell of ammonia is experienced after the appearance of the flame. The reactions are very violent, including projections outside the dish for U1 and U2. The apparent volume of U2 is much smaller than that of U0.5 and U1 (Table 1). The colour of U0.5 and U1 varies in the different parts of the as-prepared powders, revealing some heterogeneity, whereas U2 seems to be homogeneous (Table 1). Chandramouli et al.[29] suggested that in an aqueous solution of metallic nitrate and urea, the homogeneity of the solution is caused by the formation of a metal-urea complex with via the oxygen of urea. A too low urea quantity for U0.5 and U1 could explain that an initial lack of homogeneity of the solution might be reflected in the non-homogeneous colours of U0.5 and U1 as-prepared powders.

A study by Biamino et al.[28] revealed that the decomposition of urea in air releases CO_2, HCNO, H_2O and NH_3. However, the amount of the various gases will notably depend on the availability of O_2, as described in reactions (9)–(11):

$$CO(NH_2)_2 \rightarrow HCNO + NH_3 \quad (9)$$

$$HCNO + \tfrac{1}{2}O_2 \rightarrow \tfrac{1}{3}N_2 + \tfrac{1}{3}NH_3 + CO_2 \quad (10)$$

$$NH_3 + \tfrac{3}{4}O_2 \rightarrow \tfrac{1}{2}N_2 + \tfrac{3}{2}H_2O \quad (11)$$

The authors[28] further showed that when urea is mixed with a nitrate, part of the urea decomposes before the combustion reaction starts, which implies that this reaction will take place in fuel-lean conditions. In this case, the NH_3 (from (9) and possibly (10)) will be available in a too low amount to fully react with the NO_2 (produced by (5)) according to reaction (12):

$$4NO_2 + 2NH_3 \rightarrow 3N_2 + 3H_2O + \tfrac{5}{2}O_2 \quad (12)$$

Consequently, one may expect to observe red fumes characteristic of NO_2 during the nitrate/urea combustion in fuel-lean mixtures. However, regardless of the urea proportion, no red fumes were observed here, indicating that the decomposition of urea prior to combustion is subordinate. For the same reason, the NH_3 that could be produced by urea hydrolysis according to:

$$CO(NH_2)_2 + H_2O \rightarrow CO_2 + 2NH_3 \quad (13)$$

at about 80 °C, i.e. at a temperature much lower than the combustion temperature, is also negligible. Hence, the global combustion process is a combination of reactions (5) and (10) (the redox reaction), reaction (12) and, if the O_2 and NH_3 quantities are sufficient, reaction (11). If the latter does not occur, NH_3 will be in excess and the characteristic smell will be apparent.

For U0.5, with the lowest quantity of urea, the O_2 amount produced by reaction (12) is much higher than required and the global reaction may be written as:

$$2M(NO_3)_3 + \tfrac{5}{2}NH_3 + \tfrac{5}{2}HCNO \rightarrow M_2O_3 + \tfrac{11}{2}N_2 + 5H_2O + \tfrac{5}{2}CO_2 + \tfrac{15}{2}O_2 \quad (14)$$

For U1, which uses the so-called stoichiometric proportions between nitrates and urea, the global reaction is:

$$2M(NO_3)_3 + 5NH_3 + 5HCNO \rightarrow M_2O_3 + 8N_2 + 10H_2O + 5CO_2 \quad (15)$$

For U2, with the highest quantity of urea, the amount of O_2 produced by reaction (12) is not enough, reaction (11) is not

complete, and a characteristic smell of NH_3 is discernible. The global reaction becomes:

$$2M(NO_3)_3 + 10HCNO \rightarrow M_2O_3 + 8N_2 + 10H_2O + 5CO_2 \quad (16)$$

As opposed to CA combustion, there are no residual carbon species in the as-prepared powders by ureic combustion, possibly because the maximum temperature reached during the combustion is much higher for the latter procedure. The quantity of gas products as obtained from the global reactions (14)–(16), i.e. 16.75, 23 and 33 mol for U0.5, U1 and U2, respectively, could explain that the apparent volumes for powders U0.5 and U1 are much larger than that for CA powders (Table 1). However, for powder U2, the reaction is extremely violent so that foaming before appearance of the flame does not occur and the as-prepared powder is very dense.

3.1.3. Combustion using a mixture of citric acid and urea (CAU powders)

During the combustion synthesis using mixtures of CA and urea, some of the characteristics of both the CA and the ureic combustion are observed, except the appearance of a flame. Particularly, the reaction is less violent than for urea combustion, red fumes reveal the emanation of NO_2 and incandescence during a few minutes is observed. But, the most particular characteristic of CAU combustion is that foaming can be very strong. This finding is surprising since, as reported above, foaming occurs only for ureic combustions, while for CAU combustion it is observed to increase with increasing CA/U ratio.

During the combustion synthesis of CAU1 (50% CA + 50% U), the solution thickens and blackens, the foaming occurs, releasing red fumes. The as-prepared powder has an apparent volume (3v) similar to that of U0.5 and U1 and does not contain black residues (Table 1).

The synthesis of CAU2b uses the same proportion of CA and urea (50% CA + 50% U) but the ratio Φ_e is double ($\Phi_e = 2$) (Table 1). The solution blackens (no thickening is observed), then a large foaming occurs, and no red fumes are released (Table 1). So, increasing Φ_e could result in an enhancement of the foaming by limiting the thickening of the solution and also could avoid NO_2 formation. The as-prepared powder has an apparent volume (4v) larger than for CAU1. The colour, light yellow, of the powder is similar to CA0.5 and CA1 and containing black residues as well (Table 1).

The ratio $\Phi_e = 2$ was retained for CAU2a and CAU2c, but the CA/U ratio was varied (Table 1). For CAU2a (75% CA + 25% U), there was no thickening of the solution whereas red fumes were observed. The foaming and the apparent volume are significantly larger than for CAU2b (Table 1). Thus, compared to CAU2b, increasing the CA/U ratio results in the appearance of red fumes and a larger apparent volume. For CAU2c (25% CA + 75% U), there was no thickening of the solution and no red fumes, but the smell of NH3 was detected (Table 1). The as-prepared powder was yellow without black residues. The foaming and the apparent volume are smaller than for CAU2a and CAU2b. These are the consequences of the decrease the CA/U ratio compared to CAU2b.

In summary, increasing Φ_e avoids the thickening of the solution; red fumes appear when the urea quantity is insufficient, and foaming is promoted firstly by the increase in the CA/U ratio and secondly by increasing Φ_e. Since the characteristics of these combustions are not intermediate between those observed for CA and ureic combustions, we infer that there are some reactions between the intermediate products of the thermal decomposition of CA and urea (reactions (2), (3), (9) and (10), respectively). Particularly, the main influence of using a mixture of CA and urea comes from reaction between $C_5H_4O_3$ and NH_3, namely:

$$C_5H_4O_3 + NH_3 \rightarrow C_5H_5NO_2 + H_2O \quad (17)$$

Then, the carbonaceous product $C_5H_5NO_2$ would be oxidised in two steps, according to the following reactions:

$$C_5H_5NO_2 + \tfrac{3}{2}O_2 \rightarrow C_4H_3NO_2 + CO_2 + H_2O \quad (18)$$

$$C_4H_3NO_2 + \tfrac{7}{4}O_2 \rightarrow 4CO + \tfrac{3}{2}H_2O + \tfrac{1}{2}N_2 \quad (19)$$

Depending on the quantity of O_2 available, these reactions are more or less completed and CO can or not be oxidised to CO_2 in the reaction:

$$CO + \tfrac{1}{2}O_2 \rightarrow CO_2 \quad (20)$$

The combustion reaction for CAU1 can be detailed as follows. First reaction (17) takes place. Subsequently, different redox reactions occur at the same time: between $C_5H_5NO_2$ and metal nitrates ((5) and (18)), between HCNO and metal nitrates ((5) and (10)), and finally between NH_3 and NO_2 (12). The NH_3 amount produced by reactions (9) and (10) is insufficient to complete reaction (12), resulting in the emission of NO_2 as evidenced by the red fumes (Table 1). The amount of O_2 produced by reaction (12) can complete reaction (19), as shown by the absence of carbonaceous components in the product, but it remains insufficient to complete reaction (20) and thus the gas product is supposed to contain some CO. So, the global reaction for CAU1 can be written as:

$$2M(NO_3)_3 + \tfrac{5}{6}C_5H_4O_3 + \tfrac{5}{2}NH_3 + \tfrac{5}{2}HCNO \rightarrow M_2O_3 + 5N_2 + 1NO_2 + 6.67H_2O + 4.67CO_2 + 2CO \quad (21)$$

As for the combustion process involving CAU2a, the initial reaction is (17). Subsequently, redox reactions between $C_5H_5NO_2$ and metallic nitrates ((5) and (18)), and between HCNO and metal nitrates ((5) and (10)), occur at the same time. The NH_3 quantity produced by reaction (9) is insufficient to complete reaction (17) and likewise the NH_3 produced by reaction (10) to complete reaction (12). This results in the emission of NO_2. The little O_2 produced by reaction (12) can react according to (10) and (18), but is insufficient to complete these reactions, which results in large amounts of black residues. Reaction (12) cannot occur again because NO_2 already left and NH_3 is released, but in a too low quantity to be detected. So the global

reaction for CAU2a is as follows:

$$2\,M(NO_3)_3 + \tfrac{5}{2}C_5H_4O_3 + \tfrac{5}{2}NH_3 + \tfrac{5}{2}HCNO \rightarrow M_2O_3 + 1.46\,N_2 + 5\,NO_2 + 3.96H_2O + 2.83CO_2 + 0.21NH_3 + 0.37HCNO + 1.79C_5H_5NO_2 + 0.71C_4H_3NO_2 \quad (22)$$

The combustion reaction for CAU2b starts off like the one for CAU2a. However, the amount of NH_3 produced by reactions (9) and (10) is sufficient to reduce all NO_2 in reaction (12), as confirmed by the absence of red fumes. The amount of O_2 produced by (12) is adequate to complete reactions (10) and (18), and some even remains present to react with NH_3 according to reaction (11). However, this reaction cannot be completed and consequently a minor excess of NH_3, apparently too small to be perceptible, is released by reaction (10). Further, there is no longer any O_2 available to react with $C_4H_3NO_2$ according to (19), explaining the presence of black residues. The global reaction for CAU2b can thus be written as:

$$2M(NO_3)_3 + \tfrac{5}{3}C_5H_4O_3 + 5NH_3 + 5HCNO \rightarrow M_2O_3 + 6.33N_2 + 8.33H_2O + 6.67CO_2 + 1.67NH_3 + 1.67C_4H_3NO_2 \quad (23)$$

ForCAU2c the unreacted NH_3 is much more abundant than for CAU2b and therefore its distinct smell is obvious. The quantity of residual carbonaceous products is low and as such not manifested as black residues (Table 1). The global reaction for CAU2c is described by:

$$2M(NO_3)_3 + \tfrac{5}{6}C_5H_4O_3 + \tfrac{15}{2}NH_3 + \tfrac{15}{2}HCNO \rightarrow M_2O_3 + 7.17N_2 + 6.67H_2O + 8.83CO_2 + 5.83NH_3 + 0.83C_4H_3NO_2 \quad (24)$$

The quantity of gas products as obtained from the global reactions (21)–(24) is equal to 19.3, 13.8, 23.0 and 28.0 mol for CAU1, CAU2a, CAU2b and CAU2c, respectively. However, the apparent volume for powders CAU2a and CAU2b is significantly higher than for powder CAU2c (Table 1). Abreu et al.[25] showed that excess urea causes modifications of the gel formation in a modified Pechini method. It is thus proposed that the viscosity of the concentrated solution prior to the combustion should also be taken into account. Indeed, for the present CAU2 specimens, increasing the urea proportion (CAU2a < CAU2b < CAU2c) will result in an NH_3 excess (reactants in (17)), which could affect the formation of the gel from the solution, resulting in a lower viscosity at the beginning of the combustion. Consequently, the gases will be released easily without contributing significantly to the foaming.

3.1.4. *Conclusions regarding combustion synthesis*

The combustion synthesis using either only citric acid or only urea or a mixture of both as the fuel, and different fuel/nitrate ratios (Φ_e) were investigated. The main differences between the CA and U combustions are that the CA combustion produces

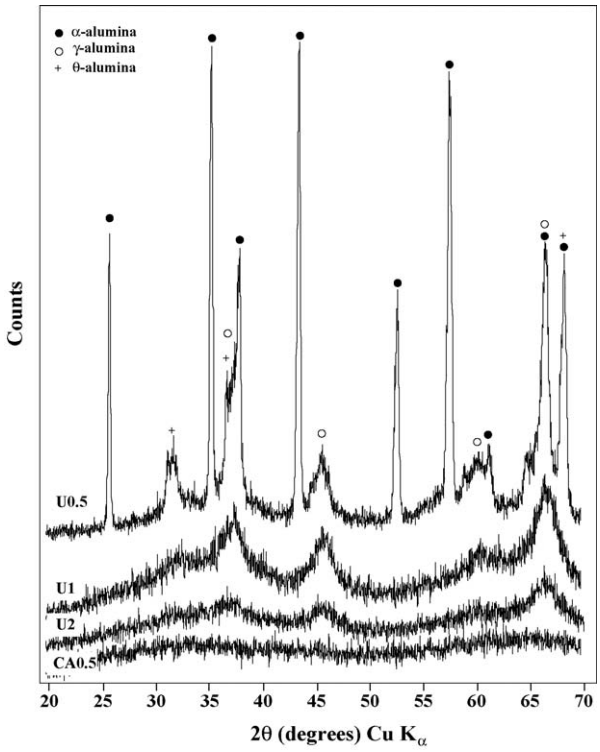

Fig. 2. Typical XRD patterns for some as-prepared powders (U0.5, U1, U2 and CA0.5). Patterns for other powders are similar to that for CA0.5.

powders that (i) contain some residual carbon species, possibly because the reaction temperature is lower, and that (ii) have a lower apparent volume, possibly because there is no foaming involved and because the quantity of gas products is lower. Using a mixture of CA and U notably produces a stronger foaming, which increases in the first place with increasing the CA/U ratio and in the second place with increasing Φ_e. It is proposed that these effects are a consequence of a combination of the occurrence of some reactions between the intermediate products of the thermal decomposition of CA and U on the one hand, and a higher viscosity at the beginning of the combustion reaction for high CA/U ratios on the other hand.

3.2. *Powder characterisation*

3.2.1. *Characterisation of the as-prepared powders*

Along the differences between the apparent volumes of powders and the presence or not of black carbonaceous residues presented in the above sections, some differences in colours have also been observed (Table 1). The basic colour of most powders is light yellow, but some powders are more intensely yellow (CAU2c) or turn towards orange (CA2), and U powders are more or less dark red and often not homogeneous (U0.5 and U1). This is probably a consequence of various degrees of chemical homogeneity and could indicate that some powders, particularly U powders, are not monophased. The XRD patterns of some as-prepared powders are reported in Fig. 2. All CA and CAU powders appear amorphous, showing patterns similar to that of CA0.5 reproduced in Fig. 2, without any observable diffraction peak. By contrast, the U0.5 pattern presents the char-

acteristic narrow peaks of the corundum structure (α-alumina), and also the very broad peaks of the cubic (mainly γ and θ alumina forms. The U1 and U2 patterns present the peaks of both the γ- and θ-forms, although the peaks are less intense for U2. Thus, the crystallisation of U powders is much more advanced than that of other powders, and the degree of crystallinity depends on the urea quantity, clearly decreasing as the ratio Φ_e increases. This finding confirms the results obtained for pure alumina.[30] For all powders, neither the α-Fe_2O_3 nor the Fe_3O_4 characteristic peaks were observed in the respective XRD patterns. However, because of the low crystallisation degree of most as-prepared samples, some phase partitioning cannot be ruled out.

DTA experiments performed in air at temperatures up to 550 °C on all the as-prepared CA and CAU powders, indicate a more or less pronounced exothermic phenomenon around 450–550 °C. This peak in the DTA curve can be associated to the combustion of the carbonaceous residues that have been observed in most CA and CAU powders (Table 1). Indeed, all black constituents have disappeared after the samples had been heated. At this stage of the investigation, all as-prepared powders were calcined in air at 550 °C before further characterisation, in order to eliminate carbonaceous contaminants. This heat treatment was observed to have no marked effect on the respective XRD patterns.

3.2.2. *Characterisation of the 550 °C-calcined powders*

The XRD patterns (not shown) of powders calcined at 550 °C were similar to those of as-prepared powders. Both SEM and specific-surface-area measurements confirm that there are substantial differences among the various powders, depending on the nature of the fuel and on the ratio Φ_e applied to the combustion synthesis.

Firstly, low-magnification SEM images (Fig. 3a–d) show that CA powders are made up of non-porous round grains, a few tens of micrometers across (CA1, Fig. 3a), whereas U powders consist of somewhat larger, veil-like grains that are very porous (U1, Fig. 3b). These differences in morphology are likely related to differences in the respective combustion processes (Table 1), which for CA powders are rather slow and without foaming, while for the U powders they are fast and with considerable volume expansion due to the production of large quantities of gasses. The CAU2a (not shown) and CAU2b (Fig. 3c) particles also exhibit a veil-like appearance, while the CAU2c grains (Fig. 3d) rather resemble those of the U powders. The distinctive morphologies for CAU2a and CAU2b can be explained by the very extensive foam development during the combustion, and as such are in agreement with the large apparent volume of the as-prepared powders (Table 1). It seems that such a morphology is obtained only when $\Phi_e = 2$, using a CA/U mixture and at the condition that the CA proportion is sufficient.

The size of the primary grains has been investigated using high-magnification SEM images (Fig. 3e–h) and correlated with both the XRD results and the specific-surface-area measurements. The grains of the U0.5 powder (Fig. 3e and f) show a heterogeneous microstructure made up of at least two more or less distinct populations or groups of particles, which are believed to be real crystallites. Some crystallites are as large as 100 nm, probably corresponding to the α-Al_2O_3 phase revealed by XRD. The second group is formed by much smaller particles, only a few nanometers large, which likely involve the cubic phases. Crystallisation into the α-form either occurred homogeneously in extended areas (Fig. 3e), or developed more locally, maybe around seeds (Fig. 3f). The expected high thermal gradients within the product during the very fast combustion reaction could explain that two crystallisation processes occur simultaneously.

The grains of the U1 powder show some mesoporosity and primary grains, generally around 10–20 nm large (Fig. 3g), but reaching 50 nm in particular regions, have developed. By contrast, for U2 a dispersion of primary grains of about 10 nm large, emerging from the grains (Fig. 3h), is noticed. The different morphology of U1 and U2 is explained by the fact that the crystallisation into the cubic forms, although observed by XRD to occur for both powders, has reached a much higher degree in the U1 powder. SEM examinations of some CA or CAU powders revealed a thinner homogeneous microstructure with meso- or micropores and crystallites of a few nanometers, which is explained by the amorphous form of these powders.

The BET specific surface areas of the powders calcined at 550 °C (S_{550}) are reported in Table 2. The S_{550} values for U0.5 and U1 (3.8 and 14.5 $m^2\ g^{-1}$, respectively) are much lower than for the other powders. This reflects the notable advancement of the crystallisation into the corundum and cubic forms for U0.5 and U1, respectively, in agreement with the XRD data. The U2 powder, prepared using twice the quantity of urea ($\Phi_e = 2$) in comparison to U1, presents a much higher S_{550} (34.3 $m^2\ g^{-1}$), consistent with a lower degree of crystallisation into the cubic forms. These values are also in good agreement with the microstructure revealed by the SEM images. Thus, for the U powders, S_{550} clearly increases when Φ_e is increased. This trend is also found for the CA powders, particularly for those having Φ_e values between 1 and 2 (44.3 and 122.8 $m^2\ g^{-1}$, respectively). The same evolution is obvious for CAU powders, except for CAU2c that, being prepared using a low CA/U ratio, rather seems to resemble U2. For CAU2a and CAU2b, the high S_{550} values (110.2 and 128.4 $m^2\ g^{-1}$, respectively) reflect the extended foaming occurring during the synthesis (Table 1) and the resulting particular morphology of very thin veil-like grains.

Table 2
BET specific surface area of the powders calcined at 550 °C (S_{550}) and calcined at 1100 °C (S_{1100})

Powder	S_{550} ($m^2\ g^{-1}$)	S_{1100} ($m^2\ g^{-1}$)
CA0.5	40.2 ± 1.2	2.3 ± 0.1
CA1	44.3 ± 1.3	1.5 ± 0.1
CA2	122.8 ± 3.7	4.0 ± 0.1
U0.5	3.8 ± 0.1	1.1 ± 0.1
U1	14.5 ± 0.4	1.7 ± 0.1
U2	34.3 ± 1.0	2.4 ± 0.1
CAU1	27.5 ± 0.8	3.7 ± 0.1
CAU2a	110.2 ± 3.3	7.8 ± 0.2
CAU2b	128.4 ± 3.3	6.2 ± 0.2
CAU2c	36.1 ± 1.1	2.7 ± 0.1

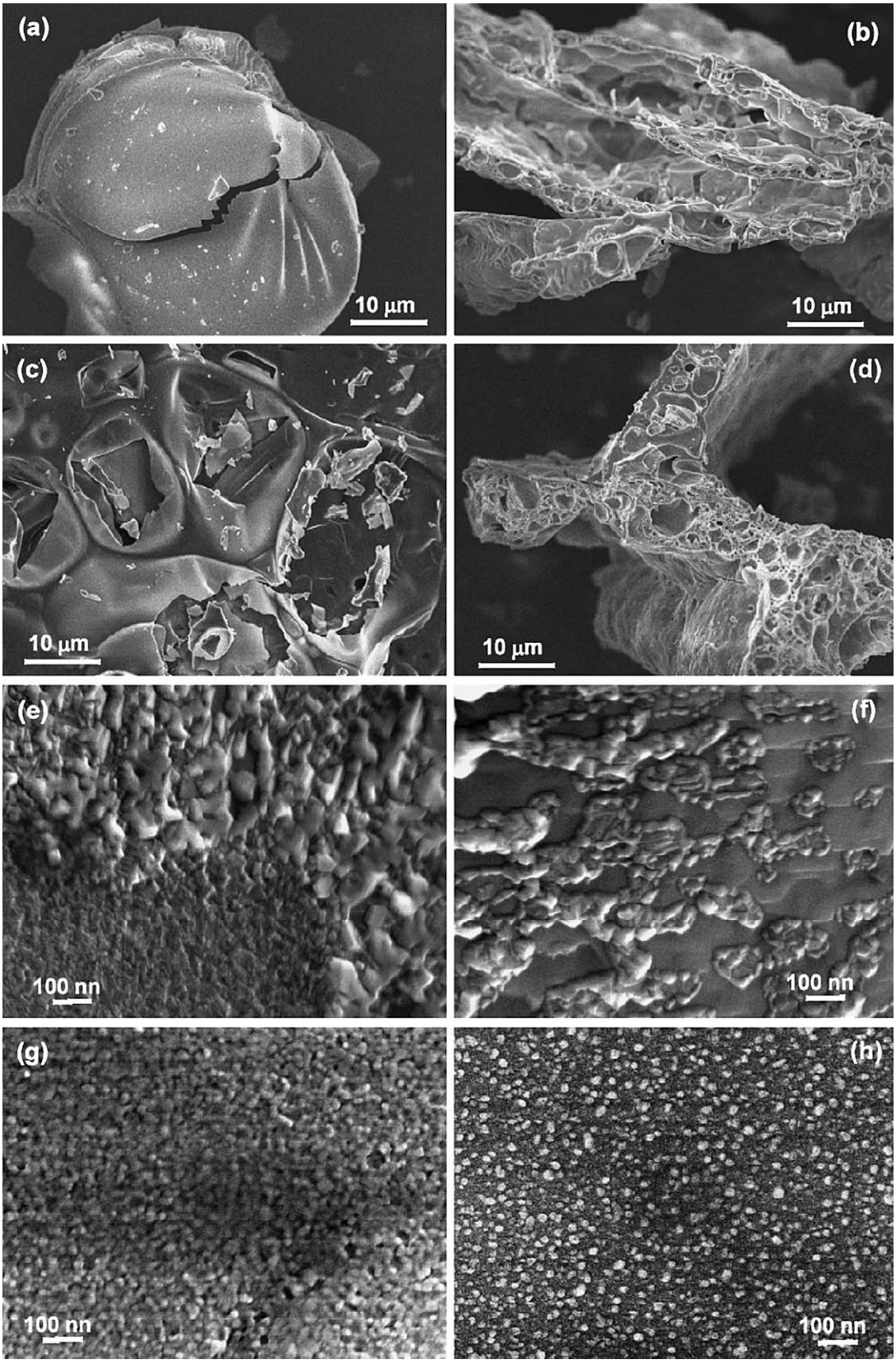

Fig. 3. FEG-SEM images at low magnification: (a) CA1; (b) U1; (c) CAU2b; (d) CAU2c and at high magnification: (e, f) U0.5; (g) U1; (h) U2. See text for details.

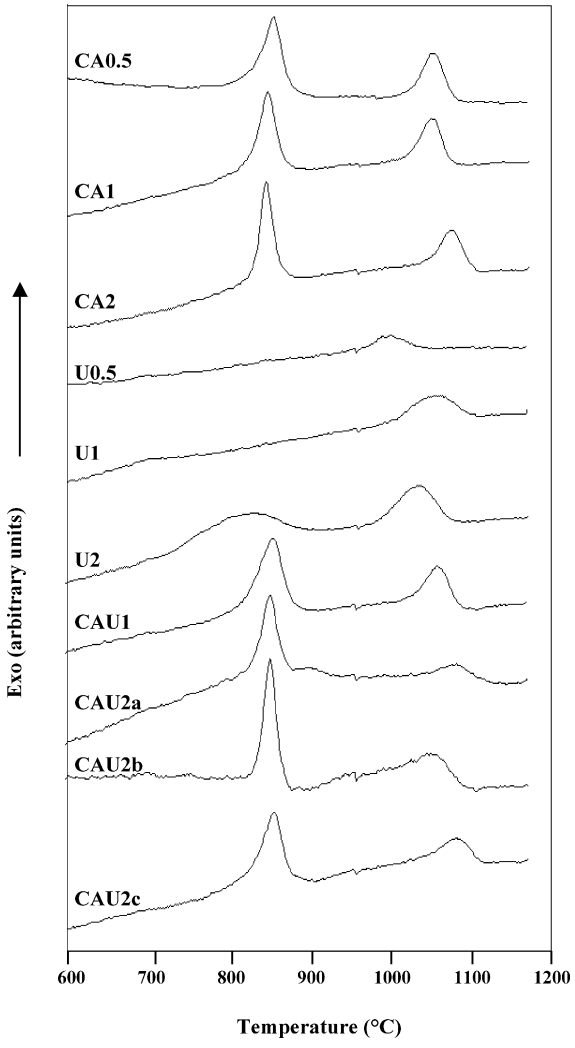

Fig. 4. DTA curves for the 550 °C-calcined powders, showing the amorphous → cubic (peak at 850–860 °C) and cubic → α (peak at 1040–1080 °C) crystallisations.

3.2.3. *DTA study of the crystallisation of the 550 °C-calcined powders*

DTA curves for the powders calcined at 550 °C were performed in air with temperature rising to 1200 °C. For all involved CA and CAU powders these curves exhibit two exothermic peaks (Fig. 4), generally at 850–860 °C and 1040–1080 °C. These peaks are attributed to the amorphous → cubic forms and θ → α transitions, respectively.[10,31] Consistently, the low-temperature peak is absent in the DTA curves of U0.5 and U1, because the corresponding as-prepared powders are already crystallised into cubic forms (Fig. 2). Moreover, as stressed above, this crystallisation phenomenon is scarcely detectable for the U2 as-prepared powder, and accordingly the corresponding DTA peak is less enhanced and shifted towards lower temperatures (about 810 °C). For most powders, the temperature of the high-temperature DTA peak, corresponding to the θ → α transition, is somewhat higher than that commonly reported for $Al_{1.8}Fe_{0.2}O_3$.[10,12–15] This disagreement may be due to the high heating rate (20 °C/min) applied in the present study, but could also reveal a better homogeneity at the atomic scale for most of the present powders, and particularly the absence of hematite seeds that are known[32] to shift the crystallisation into the corundum form towards lower temperatures. For U0.5, the high-temperature DTA peak is weaker and located at lower temperatures (around 1000 °C), most likely because the α-crystallisation is already advanced in the as-prepared sample (Fig. 2). It may thus be concluded from this DTA study that a calcination of the powders in air at 1100 °C will allow to obtaining products that are totally crystallised into the corundum form, regardless of the conditions used during the combustion synthesis. It was therefore chosen to calcine all powders at 1100 °C with a dwell time of 30 min at that temperature.

3.2.4. *Characterisation of the powders after calcination at 1100 °C*

The BET specific surface area of powders after calcination at 1100 °C (S_{1100}) are reported in Table 2 and plotted versus the corresponding S_{550} values in Fig. 5. A very large decrease of the specific surface area upon the 1100 °C calcination is observed, which is common for alumina-based powders when the crystallisation into the corundum form occurs, a process that generally involves some sintering phenomena. However, the extent of lowering differs from one powder to another. In particular, a significantly lower decrease is noticed for CA0.5, CAU1 and CAU2a than for most other powders. It should be noted that the value $S_{1100} \approx 8\ m^2\ g^{-1}$ obtained for CAU2a is relatively high for a corundum-type powder that has not been ground. On the other hand, the decrease for CA2 is higher than for most other powders.

The differences among the various samples as far as the effect of the 1100 °C calcination upon the specific surface area is concerned, are believed to result from differences in microstructural characteristics of the as-prepared powders, which in turn are determined by the combustion phenomena. Particularly, the intense foaming during the synthesis of CAU2a (Table 1), and

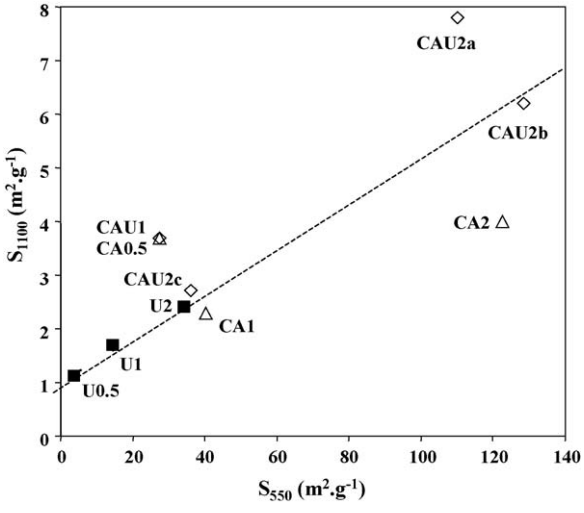

Fig. 5. The specific surface area of the powders calcined at 1100 °C (S_{1100}) vs. the specific surface area of the corresponding powders calcined at 550 °C (S_{550}) (open triangles: CA powders, full squares: U powders, open diamonds: CAU powders). The dashed line is a guide to the eye.

Table 3
Mössbauer parameters of the main ferric doublet at room temperature for the powders calcined at 1100 °C: isomer shift δ (vs. α-Fe), quadrupole splitting ΔE_Q and line width Γ (all in mm s^{-1}) and relative absorption (RA, %)

Powder	$\delta \pm 0.003$ (mm s^{-1})	$\Delta E_Q \pm 0.005$ (mm s^{-1})	$\Gamma \pm 0.003$ (mm s^{-1})	RA ± 2 (%)
CA0.5	0.289	0.540	0.352	100
CA1	0.287	0.541	0.361	100
CA2	0.289	0.547	0.360	100
U0.5[a]	0.288	0.543	0.358	79
U1[b]	0.288	0.543	0.363	96
U2	0.289	0.543	0.354	100
CAU1	0.287	0.543	0.361	100
CAU2a[c]	0.289	0.549	0.342	90
CAU2b[d]	0.288	0.534	0.330	95
CAU2c	0.300	0.530	–	100

The latter quantity equals the percentage of total iron present in this phase.
[a] Also present is a hematite sextet with hyperfine field $H_{hf} = 505.3 \pm 0.5$ kOe, $2\varepsilon_Q = -0.21 \pm 0.01$, RA = 21 ± 2%.
[b] Also present is a hematite sextet with hyperfine field $H_{hf} = 503.0 \pm 0.5$ kOe, $2\varepsilon_Q = -0.21 \pm 0.01$, RA = 4 ± 2%.
[c] Also present is a weak ferric doublet with ΔE_Q about 1.3 mm s^{-1}, RA = 10 ± 2%.
[d] Also present is a weak ferric doublet with ΔE_Q about 1.3 mm s^{-1}, RA = 5 ± 2%.

to a lesser extent in the case of CAU2b, leads to the exceptional morphology of very thin veil-like grains (Fig. 2), which likely opposes the tendency to sintering upon calcinations, unlike powders consisting of more spherically shaped particles. These results infer that, during the combustion synthesis, the choice of the fuel composition and of Φ_e is crucial to control the specific surface area of the obtained powders, even after thermal treatment to promote crystallisation.

Mössbauer spectra (MS) were recorded at room temperature for all powders calcined at 1100 °C. The relevant Mössbauer parameters are listed in Table 3. Also, MS were obtained at 80 K for CAU2a and CAU2c, but these did not provide additional information. The spectra generally, could be adequately fitted with a ferric quadrupole doublet (example for CA0.5 in Fig. 6a). However, some samples required either an additional sextet (e.g. U0.5, see Fig. 6b) or an additional weak ferric doublet (e.g. CAU2b, see Fig. 6c). The dominant doublet with $\Delta E_Q \approx 0.54$ mm s^{-1}, represents Fe^{3+} ions substituting for Al^{3+} ions in an alumina-rich corundum (α_1) lattice, in agreement with previous studies[33] on powders with the same composition prepared by the oxalate route. The weak sextet that appears in the MS of U0.5 and U1 reveals the presence of a hematite phase in the respective samples. The hyperfine field H_{hf} of the sextet (about 505 kOe) is low, compared with about 517 kOe for pure bulk hematite. This field reduction is most likely due to an Al^{3+}-for-Fe^{3+} substitution. The presence of this hematite-rich phase (α_2) indicates some phase partitioning for U0.5 and U1. A weak second doublet was required for the analysis of CAU2a and CAU2b powders (RA about 10 and 5%, respectively, quadrupole splitting $\Delta E_Q \approx 1.3$ mm s^{-1} and isomer shift close that of dominant doublet). The weak doublet was also clear in the 80 K MS of CAU2a. The large ΔE_Q value is indicative of

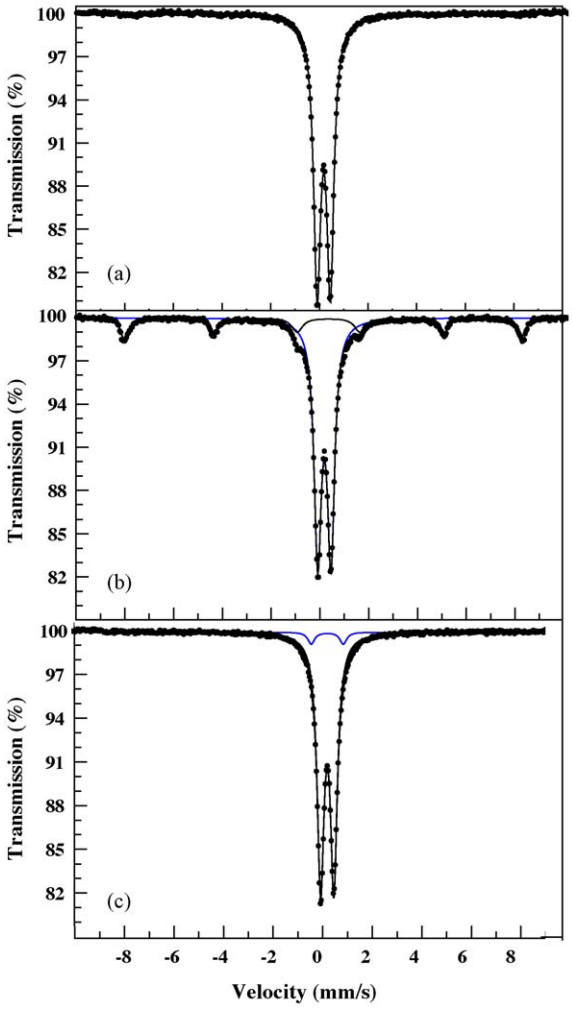

Fig. 6. Typical room temperature ^{57}Fe Mössbauer spectra showing the dominant ferric doublet detected for all powders (a) CA0.5) with either an additional sextet for (b) U0.5) or an additional weak ferric doublet (c) CAU2b). The dominant doublet represents Fe^{3+} ions substituting for Al^{3+} ions in an alumina-rich corundum lattice. The sextet reveals a hematite-phase type. The high quadrupole splitting of the weak ferric doublet reveals a strongly deformed site. See text for details.

a strongly deformed site. However, no further conclusions with respect to the involved ferric phase/site can be inferred.

The XRD patterns of the powders after calcination at 1100 °C show that the alumina-rich (α_1) phase is the dominant phase in all powders. Fig. 7 shows a zoom-in on these of patterns to facilitate detection of the possible presence of the hematite-rich (α_2) phase. From this, it is obvious that the weak hematite diffraction lines clearly appear for the U0.5 and U1 powders, in agreement with the MS analyses. Very weak α_2 peaks seem to present for other powders with $\Phi_e = 0.5$ and 1 as well, although this phase was not observed in their MS. These results show that phase partitioning could not be avoided when using $\Phi_e < 2$ for the combustion synthesis.

The lattice parameters of all 1100 °C calcined powders have been calculated from the XRD data and compared to the lattice parameters calculated from the Végard's law for the α-$Al_{1.8}Fe_{0.2}O_3$ solid solution (Fig. 8). For the later calculation, we

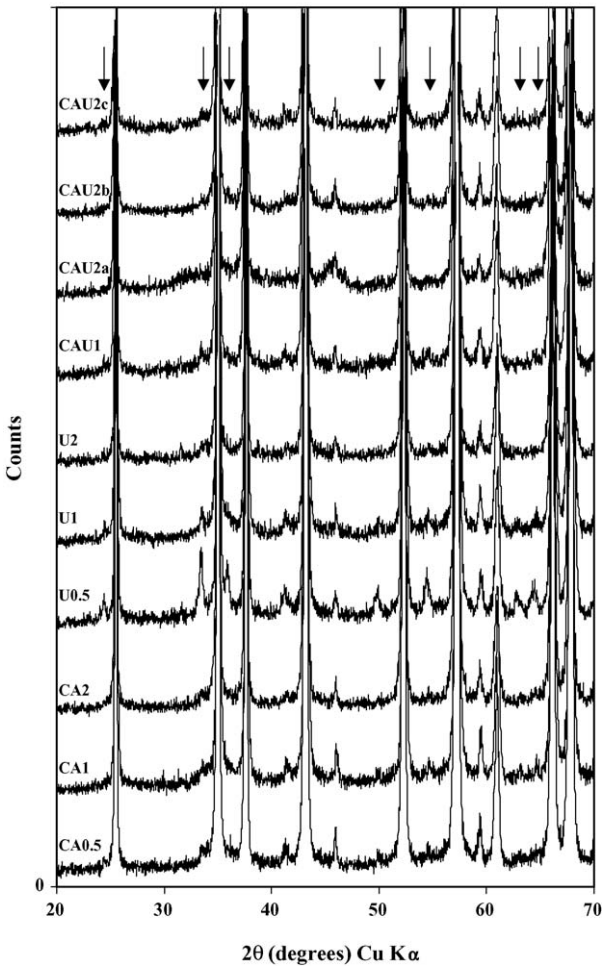

Fig. 7. XRD patterns of the powders calcined at 1100 °C.

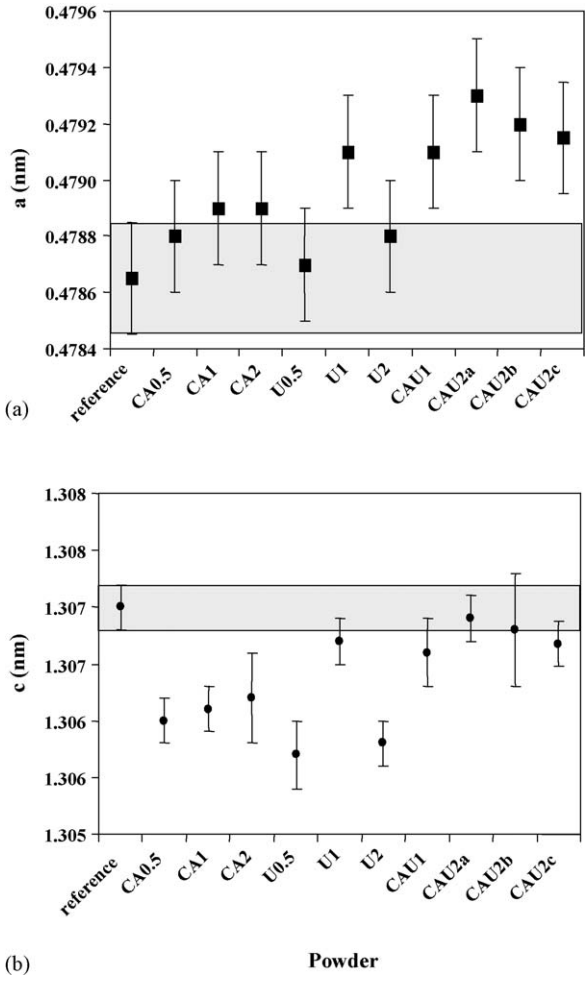

Fig. 8. (a) Cell parameter a and (b) cell parameter c, as calculated from XRD patterns of the powders calcined at 1100 °C. The reference values were calculated using the lattice parameters of α-Al_2O_3 and α-Fe_2O_3 powders prepared by the combustion route, using the same conditions as for of CAU2c, and calcined at 1100 °C. The greyed areas are guides to the eye, showing the reference values throughout the graph.

used the lattice parameters of α-Al_2O_3 and α-Fe_2O_3 powders prepared by the combustion route, using the same conditions as for of CAU2c, and calcined at 1100 °C. Regarding the unit-cell parameter *c*, only powders U1, CAU1, CAU2a, CAU2b and CAU2c follow Végard's law, while for *a*, only CA0.5, U0.5 and U2 do so. Hence, for none of the ten powders presently investigated the unit-cell parameters both obey Végard's law. In case the deviations were due to a partial phase partitioning, one would expect both *c* and *a* to be lower than the respective values for α-$Al_{1.8}Fe_{0.2}O_3$, tending rather towards the values for α-$Al_{1.9}Fe_{0.1}O_3$ ($a = 0.4773$ nm and $c = 1.3033$ nm). Some *c* values are indeed lower than the theoretical ones, but most of the *a* values are significantly higher than the theoretical ones. Moreover, these deviations are not correlated to the partitioning as detected by MS or XRD (U0.5, U1 and U2 powders). For the sake of comparison, ten α-$Al_{1.9}Fe_{0.1}O_3$ powders were prepared using the same conditions as those applied for the powders presently reported on. A positive deviation to Végard's law for the *a* parameters was also found for these powders. It is proposed that the positive deviation from Végard's law, which is clearly demonstrated for the *a* parameter, is a consequence of remaining strains in the lattice. This could also explain the negative deviation to Végard's law for the *c* parameter. In fact, the solid solution lattice seems to be constrained under compression in the *c* direction, which leads to a slight increase of the *a* parameter. This effect is more or less pronounced, depending on the experimental conditions used for the combustion synthesis. The residual stresses could favour the stabilisation of the α-$Al_{1.8}Fe_{0.2}O_3$ solid solution at room temperature.

4. Summary and conclusions

This work reports for the first time the synthesis of the metastable α-$Al_{1.8}Fe_{0.2}O_3$ solid solutions starting from precursors that were prepared by the nitrate/fuel combustion synthesis route. Three different fuels were considered: citric acid (CA powders), urea (U powders), or a mixture of both (CAU powders). In addition, different fuel/nitrate ratios (Φ_e) were applied. In the first part of this work, the reactions occurring with each synthesis were discussed, assessing the role of the possible reactions between the intermediate products of the thermal decomposition of CA and U, and of the influence of the higher viscosity

at the beginning of the combustion reaction for high CA/U ratios. Knowing and understanding these global reactions have made it possible to give a qualitative explanation for the observed differences in powder volume, morphology, crystallisation state and specific surface area, as reported in the second part of the study.

All CA and CAU as-prepared powders appear to be amorphous, whereas for U powders crystallisation into cubic and corundum forms of alumina is at an advanced stage, the more so for decreasing Φ_e. However, the CA and CAU as-prepared powders contain some residual carbon species, which could correspond to intermediate species of the CA decomposition ($C_4H_2O_3$ and $C_5H_4O_3$). All powders were therefore submitted to calcination at 550 °C prior to further investigations, in order to eliminate all carbon contamination.

The as-prepared U powders are made up of large, very porous, veil-like grains with primary grain size decreasing with increasing Φ_e (from 100 for U0.5 to 10 nm for U2). The specific surface area (S_{550}) increases accordingly. These data reflect the advanced degree of crystallisation at this stage. By contrast, the as-prepared CA powders consist of non-porous three-dimensional grains, with dimensions of a few tens of micrometer, containing meso- or micropores and crystallites of a few nanometers large. The S_{550} values are significantly higher, in particular for CA2 ($122.8\,m^2\,g^{-1}$). The microstructure of the CAU powders tends to resemble that of the U powders, but for the higher CA/U ratios (CAU2a and CAU2b), the veil-like grains are very thin. These findings may be explained by the different ways the combustion proceeds under the different experimental conditions, notably the very large foaming which occurs for some CAU combustions.

In a third part of this investigation, the powders were further calcined at 1100 °C in order to obtain the corundum form. A combination of Mössbauer spectroscopy and XRD revealed that only the powders prepared with $\Phi_e = 2$ are the desired single-phase α-$Al_{1.8}Fe_{0.2}O_3$ solid solutions. Negative and positive deviations to Végard's law are generally observed for the *c* and *a* unit-cell parameters, respectively, which could be a consequence of remaining strains in the lattice. The residual stresses could favour the stabilisation of the α-$Al_{1.8}Fe_{0.2}O_3$ solid solution at room temperature. Finally, it was found that the powders prepared with $\Phi_e = 2$ and with either pure CA (CA2) or the higher CA/U ratios (75/25 and 50/50 for CAU2a and CAU2b, respectively) have retained the higher specific surface area, the highest being for CAU2a with $S_{1100} = 7.8 \pm 0.2\,m^2\,g^{-1}$, which is relatively high for a corundum-type powder which has not been mechanically ground. Although the present work was restricted to a particular composition, it can be generalised to samples with a lower iron content. The results on the synthesis of carbon nanotubes using such powders as catalysts will be reported elsewhere.

References

1. Bye, G. C. and Simpkin, G. T., Influence of Cr and Fe formation of α-Al_2O_3 from γ-Al_2O_3. *J. Am. Ceram. Soc.*, 1974, **57**, 367–371.
2. Walker, J. S., Straguzzi, G. I., Manogue, W. H. and Schuit, G. C. A., Carbon monoxide and propene oxidation by iron oxides for auto-emission control. *J. Catal.*, 1988, **110**, 298–309.
3. Peigney, A., Laurent, Ch., Dobigeon, F. and Rousset, A., Carbon nanotubes grown in situ by a novel catalytic method. *J. Mater. Res.*, 1997, **12**, 613–615.
4. Laurent, Ch., Peigney, A., Dumortier, O. and Rousset, A., Carbon nanotubes-Fe-alumina nanocomposites. Part II. Microstructure and mechanical properties of the hot-pressed composites. *J. Eur. Ceram. Soc.*, 1998, **18**, 2005–2013.
5. Peigney, A., Laurent, Ch., Flahaut, E. and Rousset, A., Carbon nanotubes as a part of novel ceramic matrix nanocomposites. *Ceram. Int.*, 2000, **26**, 677–683.
6. Flahaut, E., Peigney, A., Laurent, Ch., Marlière, Ch., Chastel, F. and Rousset, A., Carbon nanotube-metal-oxide nanocomposites: microstructure, electrical conductivity and mechanical properties. *Acta Mater.*, 2000, **48**, 3803–3812.
7. Peigney, A., Laurent, Ch., Dumortier, O. and Rousset, A., Carbon nanotubes-Fe-alumina nanocomposites. Part I. Influence of the Fe content on the synthesis of powders. *J. Eur. Ceram. Soc.*, 1998, **18**, 1995–2004.
8. Laurent, Ch., Peigney, A. and Rousset, A., Synthesis of carbon nanotubes-Fe-alumina nanocomposite powders by selective reduction of different $Al_{1.8}Fe_{0.2}O_3$ solid solutions. *J. Mater. Chem.*, 1998, **8**, 1263–1272.
9. Muan, A. and Gee, C. L., Phase equilibrium studies in the system iron oxide-Al_2O_3 in air and at 1 Atm pressure. *J. Am. Ceram. Soc.*, 1956, **39**, 207–214.
10. Rousset, A. and Paris, J., Formation des solutions solides binaires et ternaires des sesquioxydes de chrome, d'aluminium et de fer. III. Le système Fe_2O_3-Al_2O_3. *Bull. Soc. Chim. Fr.*, 1972, **10**, 3729–3733.
11. Meyers, C. E., Mason, T. O., Petuskey, W. T., Halloran, J. W. and Bowen, H. K., Phase equilibria in the system Fe-Al-O. *J. Am. Ceram. Soc.*, 1980, **63**, 659–663.
12. Devaux, X., Laurent, Ch. and Rousset, A., Chemical synthesis of metal nanoparticles dispersed in alumina. *Nanostruct. Mater.*, 1993, **2**, 339–346.
13. Popovic, S., Ristic, M. and Music, S., Formation of solid solution in the system Al_2O_3-Fe_2O_3. *Mater. Lett.*, 1995, **23**, 139–142.
14. Tartaj, P. and Tartaj, J., Microstructural evolution of iron-doped alumina nanoparticles synthesized from microemulsion. *Chem. Mater.*, 2002, **14**, 536–541.
15. Polli, A., Lange, F. F., Levi, C. G. and Mayer, J., Crystallisation behavior and microstructure evolution of (Al, Fe)$_2O_3$ synthezed from liquid precursors. *J. Am. Ceram. Soc.*, 1996, **79**, 1745–1755.
16. Patil, K. C., Aruna, S. T. and Minami, T., Combustion synthesis an update. *Curr. Op. Sol. St. Mater. Sci.*, 2002, **6**, 507–512.
17. Specchia, S., Civera, A. and Saracco, G., In situ combustion synthesis of Perovskite catalysts for efficient and clean methane premixed metal burners. *Chem. Eng. Sci.*, 2004, **59**, 5091–5098.
18. Li, F., Hu, K., Li, J., Zhang, D. and Chen, G., Combustion synthesis of γ-lithium aluminate by using various fuels. *J. Nucl. Mater.*, 2002, **300**, 82–88.
19. Civera, A., Pavese, M., Saracco, G. and Specchia, S., Combustion synthesis of Perovskite-type catalysts for natural gas combustion. *Catal. Today*, 2003, **83**, 199–211.
20. Li, W., Li, J., Guo, J. and Synthesis, Characterisation of nanocrystalline $CoAl_2O_4$ spinel powder by low temperature combustion. *J. Eur. Ceram. Soc.*, 2003, **23**, 2289–2295.
21. Zhang, Y. and Stangle, G. C., Preparation of fine multicomponent oxide ceramic powder by a combustion synthesis process. *J. Mater. Res.*, 1994, **9**, 1997–2004.
22. Kingsley, J. J. and Pederson, L. R., Energetic materials in ceramics synthesis. *Mater. Res. Soc. Symp. Proc.*, 1993, **296**, 361–366.
23. Patil, K. C., Advanced ceramics combustion synthesis and properties. *Bull. Mater. Sci.*, 1993, **16**, 533–541.
24. Pathak, L. C., Singh, T. B., Das, S., Verma, A. K. and Ramachandrarao, P., Effect of pH on the combustion synthesis of nano-crystalline alumina powder. *Mater. Lett.*, 2002, **57**, 380–385.
25. Abreu Jr., A., Zanetti, S. M., Oliviera, M. A. and Thim, G. P., Effect of urea on lead zirconate titanate-Pb($Zr_{0.52}Ti_{0.48}O_3$)- nanopowders synthesized by the Pechini method. *J. Eur. Ceram. Soc.*, 2005, **25**, 743–748.

26. Hon, Y. M., Fung, K. Z. and Hon, M. H., Synthesis characterization of $Li_{1+}Mn_{2-}O_4$ powders prepared by citric acid gel process. *J. Eur. Ceram. Soc.*, 2001, **21**, 515–522.
27. Pacewska, B. and Keshr, M., Thermal transformations of aluminium nitrate hydrate. *Thermochim. Acta*, 2002, **385**, 73–80.
28. Biamino, S. and Badini, C., Combustion synthesis of lanthanum chromite sartting from water solutions: investigation of process mechanism by DTA-TGA-MS. *J. Eur. Ceram. Soc.*, 2004, **24**, 3021–3034.
29. Chandramouli, V., Anthonysamy, S. and Rao, P. R. V., Combustion synthesis of Thoria—a feasibility study. *J. Nucl. Mater.*, 1999, **265**, 255–261.
30. Bhaduri, S., Zhou, E. and Bhaduri, S. B., Auto ignition processing of nanocrystalline α-Al_2O_3. *Nanostruct. Mater.*, 1996, **7**, 487–496.
31. Clar, C., Scian, A. N. and Aglietti, E. F., Synthesis and characterization of aluminum carboxylate gels. *Thermochim. Acta*, 2003, **407**, 33–40.
32. McArdle, J. L. and Messing, G. L., Transformation and microstructure control in boehmite-derived alumina by ferric oxide seeding. *Adv. Ceram. Mater.*, 1988, **3**, 387–392.
33. Peigney, A., Coquay, P., Flahaut, E., Vandenberghe, R. E., De Grave, E. and Laurent, Ch., A study of the formation of single- and double-walled carbon nanotubes by a CVD method. *J. Phys. Chem. B*, 2001, **105**, 9699–9710.